LAWRENCE
LIVERMORE
NATIONAL
LABORATORY

LLNL-BOOK-676295

Collisional-Radiative Modeling for Radiation Hydrodynamics

H. A. Scott

August 14, 2015

Modern Methods in Collisional-Radiative Modelling of Plasmas

Disclaimer

Collisional-Radiative Modeling for Radiation Hydrodynamics Codes

Howard A. Scott

Lawrence Livermore National Laboratory

Abstract

Collisional-radiative models are used to provide material data to radiation hydrodynamics codes to model non-equilibrium conditions. Coupling the atomic kinetics to hydrodynamics and radiation transport presents multiple challenges, ranging from providing the required information over a wide range of conditions to maintaining energy conservation and numerical stability. We discuss some of the physical and numerical issues that arise and present modifications and extensions to the usual collisional-radiative formalism to address these issues.

1. Introduction

Collisional-radiative (CR) models provide a detailed description of the behavior of atoms (and molecules) in plasmas over a wide range of conditions. They have proven to be very useful tools for diagnosing plasma properties by analyzing emission spectra, but their utility extends far beyond this task. Inherent in the detailed description of level occupations and transition rates is the information underlying the basic material properties used in radiation hydrodynamics (RH) codes. Evaluating the material radiative properties (absorption and emission coefficients) and equation of state (EOS) with a CR model then extends the applicability of a RH code into regimes where the assumption of local thermodynamic equilibrium (LTE) is not valid, enabling modeling of a wider range of laboratory and astrophysical plasmas.

Applying CR models within a RH code presents multiple challenges. RH simulations of laboratory experiments often include many materials and span wide ranges in density and temperature. The CR model for each individual element included must then cover all charge states that may be accessed during the simulation. Computational efficiency becomes a major concern, so most RH simulations have used highly averaged models. Additionally, CR models must remain valid over the wide range of non-LTE conditions encountered during many simulations, including high-density conditions where effects such as electron degeneracy and ionization potential depression (IPD) become important. Incorporating these effects into the CR model is straightforward in some aspects, but problematic in others.

Hydrodynamic and radiation transport calculations require not only basic material properties – energy density and pressure for hydrodynamics, absorption/emission coefficients for radiation transport – but also material responses, i.e. derivatives. When LTE applies, the required derivatives are usually those with respect to temperature and density. In the more general non-LTE case, other derivatives, e.g. with respect to photon intensities, may also prove useful. Fortunately, a straightforward extension of the CR solution provides most derivatives with little additional computational effort. The difficulties here lie in adapting algorithms in the RH code to use non-LTE material responses. In particular, radiation transport often depends quite strongly on material response and handling the full non-LTE response significantly complicates solution algorithms.

More subtle challenges arise from considering discretization effects. Maintaining energy conservation in a RH simulation with both EOS and radiative properties provided by CR models demands consistency in the discretized equations, reflecting the fact that the same microphysics is responsible for both types of material properties. Discretization in time and photon frequency affects accuracy and energy conservation in a manner only slightly more complicated than that of a corresponding LTE simulation. Discretization of energy levels in the CR model

affects energy conservation in a less obvious manner and can produce inconsistencies in radiative properties or energy balance.

There are definite limitations on RH simulations using CR models. It is not feasible for an in-line CR evaluation to incorporate all the physics required for deriving detailed material properties, especially outside the weakly coupled, low density plasma regime. Nor is it realistic to expect that an in-line CR evaluation can provide the fidelity achieved by dedicated LTE opacity and EOS codes. However, using material and radiative properties from even highly approximate non-LTE models is preferable to using the best LTE information when LTE is a poor approximation. The philosophy espoused here is to use the best affordable CR models in the RH simulation, while taking care to avoid discretization effects as much as possible, to most accurately model the overall evolution of mass and energy. If desired, more involved CR models can be utilized afterwards in a post-processing mode to check consistency or obtain detailed spectral predictions.

The following section presents the basic formalism and material properties considered in this chapter. Extensions of the basic formalism for calculating derivatives are presented in section 3, along with comments about utilizing the derivatives in a RH code. Incorporating two high-density effects, ionization potential depression and electron degeneracy, into a CR model is addressed in section 4. Section 5 analyzes effects arising from discrete photon frequencies and energy levels, while section 6 then discusses issues arising from time discretization and operator splitting in the context of a radiation transport simulation.

2. Governing equations

The basic collisional-radiative formalism has been presented in Chapter 1. We repeat it here both to establish the nomenclature used in this chapter and to provide expressions used in later sections and to define basic material properties of interest. We also specify the equations used for radiation transport, for both the "thermal" radiation transport that is prevalent in RH codes and for line radiation transport.

a) Atomic kinetics

The fundamental description utilized by a CR model consists of distributions of atoms (in any possible charge state), electrons and photons. The electrons can occupy discrete bound states, enumerated with a set of atomic levels, or a continuum of unbound (free) states. Each bound state i is characterized by its population y_i, statistical weight g_i and energy E_i. The distribution of atomic populations $\mathbf{y}$ amongst the bound states is determined by the rate equation

$$\frac{d\mathbf{y}}{dt} = \mathbf{A}\mathbf{y} \tag{2.1}$$

where the rate matrix $\mathbf{A}$ includes all transitions between pairs of levels. The time derivative here is a total derivative and contains spatial transport terms. In this chapter we shall treat Eq. (2.1) in the Lagrangian context in which spatial transport terms are absent.

While we are primarily concerned here with handling a general non-LTE distribution of populations, we first state properties of the LTE distribution for a given electron temperature T_e and density n_e. Within a given charge state, the bound states obey a Boltzmann distribution

$$\frac{y_i}{y_j} = \frac{g_i}{g_j} e^{-(E_i - E_j)/kT_e} \tag{2.2}$$

while the populations of neighboring charge states are related by the Saha equation

$$\frac{N_{i+1}}{N_i} n_e = 2\left(\frac{2\pi m_e kT_e}{h^2}\right)^{3/2} \frac{Z_{i+1}(T_e)}{Z_i(T_e)} e^{-\Delta E/kT_e} \tag{2.3}$$

Here, N_i, N_{i+1} are the total populations of charge states i, $i+1$, separated by ionization potential ΔE, and

$$Z_i = \sum_{j \in \{i\}} g_j e^{-(E_j - E_j^0)/kT_e} \tag{2.4}$$

is the partition function for charge state i (with ground state energy E_j^0) with the sum running over all bound states j within charge state i.

The transition rates themselves depend on the free electron and photon distributions and also affect the local free electron distribution, as dictated by number, charge and energy conservation. In most applications of CR models, the free electrons are assumed to equilibrate quickly and are described with a thermal distribution characterized by temperature T_e. Similarly, the ions are described with a thermal distribution characterized by temperature T_i. Non-local evolution of these thermal distributions occurs within the RH code using hydrodynamics and conduction. Non-thermal electron distributions can arise from a variety of physical processes and may also be present in a RH code. Using these non-thermal distributions within a CR model is straightforward and has been addressed in [1]. Evolving these distributions in time may be important for applications with particularly short timescales [2] or low densities [3], and can be done in conjunction with a CR model [3-5]. However, in this chapter we assume the electrons are thermalized and, at low densities, are described by the Maxwellian distribution

$$f_e(\varepsilon) = n_e 4\pi \left(\frac{1}{\pi k T_e}\right)^{3/2} \varepsilon^{1/2} e^{-\varepsilon/kT_e} \tag{2.5}$$

where ε refers to the electron energy and we have assumed nonrelativistic electrons with $\varepsilon = \frac{1}{2} m_e \mathrm{v}^2$. For a plasma which is overall charge neutral, the electron density will satisfy

$$n_e = \sum_i z_i y_i \tag{2.6}$$

where z_i is the net charge associated with level i.

The collisional rate for the i→j transition of energy E_{ij} is obtained by integrating over the electron distribution f_e

$$C_{ij} = \int_{E_{ij}}^{\infty} \mathrm{v}(\varepsilon) \sigma_c^{ij}(\varepsilon) f_e(\varepsilon) d\varepsilon \tag{2.7}$$

where σ_c^{ij} is the collisional cross section as a function of electron energy ε. The inverse j→i rate can be obtained from the principle of detailed balance, which states that in equilibrium, any reaction is exactly counterbalanced by its inverse reaction (see [6] for a more detailed discussion). For an LTE population distribution and thermal electron distribution, we then have $y_i C_{ij} = y_j C_{ji}$.

Radiative transition rates can be obtained in a similar manner. The radiative rate for the i→j transition is

$$R_{ij} = 4\pi \int_0^{\infty} \sigma_\nu^{ij} J_\nu \frac{d\nu}{h\nu} \tag{2.8}$$

where σ_ν^{ij} is the radiative cross section as a function of photon frequency ν and J_ν is the angle-averaged photon intensity as described below. In equilibrium, the inverse rates satisfy $y_i R_{ij} = y_j R_{ji}$ but have both spontaneous and stimulated ($\propto J_\nu$) components

$$R_{ji} = 4\pi \left(\frac{y_i}{y_j}\right)^{LTE} \int_0^{\infty} \sigma_\nu^{ij} \left(J_\nu + \frac{2h\nu^3}{c^2}\right) e^{-h\nu/kT_e} \frac{d\nu}{h\nu} \tag{2.9}$$

For bound-bound radiative transitions, the absorption cross section is described with the profile function ϕ_{ij}

$$\sigma_\nu^{ij} = \sigma^{ij} \phi_{ij}(\nu) \ , \ \int \phi_{ij}(\nu) d\nu = 1 \tag{2.10}$$

and is usually assumed to be non-zero only in a narrow frequency range centered around $h\nu_{ij} = E_j - E_i$. In this approximation, the transition rates are given by

$$R_{ij} = \frac{4\pi}{h\nu_{ij}} \sigma^{ij} \bar{J}_{ij} \ , \ R_{ji} = \frac{g_i}{g_j} \frac{4\pi}{h\nu_{ij}} \sigma^{ij} \left(\frac{2h\nu_{ij}^3}{c^2} + \bar{J}_{ij}\right) \tag{2.11}$$

where

$$\bar{J}_{ij} = \int_0^{\infty} J_\nu \phi_{ij}(\nu) d\nu \tag{2.12}$$

The primary output from a CR model is the atomic level population distribution. The population densities, along with the CR model parameters (energy levels and transition rates) then serve as the building blocks for the basic quantities of interest for the RH code – material energy density and pressure, plus absorption and emission coefficients.

b) Material properties

For a RH code, the primary material properties of interest are the material energy density E_m and pressure P_m. Here we assume a low density plasma so that we may neglect particle interactions and use an ideal gas EOS for the thermal energy and pressure, augmented by the internal energy density due to the distribution of excited states.

$$E_m = \tfrac{3}{2} n_e k T_e + \tfrac{3}{2} n_i k T_i + E_{\text{int}} \ , \ E_{\text{int}} = \sum_i E_i y_i$$
$$P_m = n_e k T_e + n_i k T_i \tag{2.13}$$

Modifications to these expressions at high density will be considered in Sec. 4.

The absorption (α_ν) and emission (η_ν) coefficients are constructed by summing over all radiative transitions

$$\alpha_\nu = \sum_{i<j} \sigma_\nu^{ij} \left(y_i - \frac{g_i}{g_j} y_j \right) \ , \ \eta_\nu = \frac{2h\nu^3}{c^2} \sum_{i<j} \sigma_\nu^{ij} \frac{g_i}{g_j} y_j \tag{2.14}$$

where σ_ν^{ij} is the cross section at frequency ν for the i→j radiative transition and we have neglected the contribution of scattering to the emission coefficient.

If the bound states have an LTE distribution, then the absorption and emission coefficients are related by Kirchoff's law

$$\frac{\eta_\nu}{\alpha_\nu} = \frac{2h\nu^3}{c^2} \frac{1}{e^{h\nu/kT_e} - 1} = B_\nu \tag{2.15}$$

where B_ν is the Planck function.

c) Radiation transport

In contrast to ions and electrons, photons do not equilibrate quickly and can have very long mean free paths. Radiation transport methods are used to evolve the photon distribution in space and time, most commonly as an equation for the specific intensity I_ν,

$$\frac{1}{c} \frac{\partial I_\nu}{\partial t} + \vec{\Omega} \bullet \nabla I_\nu = -\alpha_\nu I_\nu + \eta_\nu = -\alpha_\nu \left(S_\nu - I_\nu \right) \tag{2.16}$$

where the second equality introduces the source function

$$S_\nu = \frac{\eta_\nu}{\alpha_\nu} \tag{2.17}$$

The specific intensity is related to the photon phase space distribution function f_γ by

$$I_\nu = \frac{2h\nu^3}{c^2} f_\gamma(\vec{r}, \nu, \vec{\Omega}, t) \tag{2.18}$$

Because of the strong coupling between the radiation and matter, the radiation transport equation is solved together with an equation describing the relevant aspect of material evolution. In RH codes that must account for significant energy transport by radiation, this is usually the material energy equation

$$\frac{dE_m}{dt} = 4\pi \int \alpha_\nu \left(J_\nu - S_\nu \right) + Q \tag{2.19}$$

where J_ν is the angle-averaged intensity

$$J_\nu = \frac{1}{4\pi} \int I_\nu \, d\Omega \tag{2.20}$$

and Q represents any additional energy sources.

In codes that are specialized to low densities, the material evolution is described directly by the CR system. In this case, the radiation in a narrow frequency range, e.g. a single strong line transition, directly couples to the level populations. The prototypical example of this type of system is the two-level atom with a single discrete radiative transition and a collisional transition. The source function for such a system, obtained under the approximation that the width of the spectral line is narrow (and assuming complete redistribution), becomes

$$S_{ij} = \frac{2h\nu_{ij}^3}{c^2} \frac{1}{\left(g_i y_j / g_j y_i \right) - 1} = (1 - \theta) \bar{J}_{ij} + \theta B_{ij} \tag{2.21}$$

where B_{ij} is the Planck function evaluated at ν_{ij} and θ depends on C_{ij} and the spontaneous component of R_{ij}.

Solution algorithms exploit the fact that S_{ij} is independent of frequency and is a linear function of $\overline{J}$. The complete source function, with contributions from overlapping line and continuum transitions, is more complicated but retains a strong dependence on $\overline{J}$ at densities low enough that collisions do not dominate the transitions from the upper level.

3. Non-LTE Material Response

A stand-alone CR calculation calculates transition rates and, from those, population distributions for a given set of physical conditions – primarily the (electron or ion) density and temperature, plus the photon distribution. The calculation may involve a time evolution of the populations, but it does not involve a time evolution of the conditions. When used within a RH code, the mass density (plus elemental concentrations) fixes the total ion densities. Evolving the mass density and temperature is a task for the RH code, or at least for equations and algorithms outside the CR structure. The rate equation is predominantly linear in the populations and most solution methods only require evaluating the rates for the single set of conditions at the beginning of each timestep. The material properties passed to a RH code are then evaluated with updated populations from the end of the (atomic kinetics) timestep. By contrast, solution methods for evolving the non-linear equations of radiation transport and hydrodynamics over a timestep typically require evaluating material properties for multiple sets of conditions or, commonly, for the conditions at the beginning of the (hydrodynamics / radiation transport) timestep along with a set of derivatives to model the response of those properties to changing conditions throughout the timestep. For example, hydrodynamic simulations typically describe the material response with an EOS, including the associated thermodynamic derivatives. Thermal radiation transport algorithms depend on the relationship between E and T, including the specific heat, while efficient line radiation transport algorithms using some form of linearization depend on derivatives with respect to $\overline{J}$.

The rate equation is only pseudolinear in the populations when trying to satisfy charge neutrality, as the electron density used to evaluate the rates itself depends on the populations. However, the non-linearity is usually quite mild and can be handled by iterating the CR calculation to converge the electron density. Solution methods for the rate equation that subdivide the timestep also may reevaluate rates with updated electron densities. In neither case do the physical conditions specified by the RH code – mass density, temperature and radiation spectrum – change between evaluations of the CR equations.

Forming derivatives of material properties dependent on the populations requires derivatives of the populations themselves. This is a crucial point, as the populations respond strongly to changes in the physical conditions. Failure to include accurate population derivatives can lead to material property derivatives that are drastically in error, severely affecting the stability and accuracy of the RH algorithms.

Fortunately, those population derivatives can be obtained without a great deal of additional effort. For example, the derivatives with respect to electron temperature can be obtained by integrating

$$\frac{d}{dt}\frac{\partial \mathbf{y}}{\partial T_e} = \frac{\partial \mathbf{A}}{\partial T_e}\mathbf{y} + \mathbf{A}\frac{\partial \mathbf{y}}{\partial T_e} \tag{3.1}$$

over a single timestep subject to the initial condition

$$\frac{\partial \mathbf{y}}{\partial T_e}(t=0) = 0 \tag{3.2}$$

Derivatives of the transition rates can be calculated at the same time as the rates themselves at a small additional cost and Eq. (3.1) can be integrated in parallel with Eq. (2.1). For instance, discretizing Eq. (2.1) with the common fully implicit single step backwards Euler method produces

$$\frac{1}{\Delta t}\left(\mathbf{y}^{n+1} - \mathbf{y}^{n}\right) = \mathbf{A}\mathbf{y}^{n+1} \Rightarrow \mathbf{y}^{n+1} = \left(\mathbf{I} - \Delta t\mathbf{A}\right)^{-1}\mathbf{y}^{n} \tag{3.3}$$

while the equation for the temperature derivative becomes

$$\frac{1}{\Delta t}\left(\frac{\partial \mathbf{y}^{n+1}}{\partial T_e} - \frac{\partial \mathbf{y}^{n}}{\partial T_e}\right) = \frac{\partial \mathbf{A}}{\partial T_e}\mathbf{y}^{n+1} + \mathbf{A}\frac{\partial \mathbf{y}^{n+1}}{\partial T_e} \Rightarrow \frac{\partial \mathbf{y}^{n+1}}{\partial T_e} = \left(\mathbf{I} - \Delta t\mathbf{A}\right)^{-1}\Delta t\frac{\partial \mathbf{A}}{\partial T_e}\mathbf{y}^{n+1} \tag{3.4}$$

Not all rates contribute to the right hand side of Eq. (3.4). For instance, radiative excitation, de-excitation and

ionization rates are not explicitly dependent on temperature or electron density, while derivatives with respect to $\overline{J}$ for a single transition result in only four non-zero entries in $\partial\mathbf{A}/\partial\overline{J}$.

It remains to relate the derivatives required by the RH code to those obtained from the CR system, which is solved at fixed ρ and J_ν. A minor complication is that the (self-consistent) temperature and electron density are not independent variables. The required derivatives can be obtained from

$$\left(\frac{\partial y_i}{\partial T}\right)_\rho = \left(\frac{\partial y_i}{\partial T}\right)_{n_e} + \left(\frac{\partial y_i}{\partial n_e}\right)_T \left(\frac{\partial n_e}{\partial T}\right)_\rho \tag{3.5}$$

$$\left(\frac{\partial y_i}{\partial \rho}\right)_T = \left(\frac{\partial y_i}{\partial \rho}\right)_{n_e} + \left(\frac{\partial y_i}{\partial n_e}\right)_\rho \left(\frac{\partial n_e}{\partial \rho}\right)_T \tag{3.6}$$

Using the fact that the CR system is linear in y_i, $\left(\partial y_i/\partial\rho\right)_{n_e} = y_i/\rho$, and we can sum Eq. (3.6) over levels using Eq. (2.6) to produce the relationship

$$\rho\left(\frac{\partial n_e}{\partial \rho}\right)_T = n_e\left[1 - \sum_i z_i \left(\frac{\partial y_i}{\partial n_e}\right)_\rho\right]^{-1} \tag{3.7}$$

which is useful in calculating the derivatives with respect to density.

A more problematic complication has to do with the fact that the physical state for the CR model is defined in terms of more variables than was true under the assumption of LTE. The derivatives measuring the response to changes in one variable with all other variables held constant from the CR calculation do not carry the same information as the corresponding derivatives from an LTE calculation. This is not problematic in calculating the derivatives with the CR model, but rather in using them in the RH code.

We illustrate this with the example of the specific heat at constant volume, $c_V = \partial\varepsilon/\partial T$, a quantity used in thermal radiation transport and potentially in many other contexts in a RH code. Consider the relationship between the material energy density E_m, the material properties and the radiation field:

$$E_m = \tfrac{3}{2}\left(n_e + n_i\right)kT + E_{\text{int}}\left(T, J_\nu, t\right) \tag{3.8}$$

Here, n_e (n_i) is the number density of the free electrons (ions), which are assumed to have a thermal distribution corresponding to the material temperature T (and we have assumed $T=T_e=T_i$ for simplicity). E_{int} is the material internal energy, which depends not only on the temperature and density, but also on the radiation field, denoted by J_ν, and on the time t. Since thermal radiation transport calculations are done at fixed mass density, all derivatives are taken at constant ρ and we then focus on the temperature and radiation field as the relevant variables.

For material in LTE, the internal energy at constant density depends only on temperature. The changes in material energy density and temperature are then related through the specific heat c_V:

$$\frac{dE_m}{dt} = c_V^{LTE}\frac{dT}{dt}\ ,\ c_V^{LTE} = \left(\frac{\partial E_m}{\partial T}\right)_{J_\nu = B_\nu} \tag{3.9}$$

Implicit in this formulation is the assumption that either radiative interactions are completely unimportant or that the radiation also has a thermal distribution, i.e. $J_\nu = B_\nu$, where B_ν is the Planck distribution. In the more general non-LTE formulation, the change of material energy density is comprised of three different types of terms:

$$\frac{dE_m}{dt} = \left(\frac{\partial E_m}{\partial T}\right)_{J_\nu}\frac{\partial T}{\partial t} + \sum_\nu\left(\frac{\partial E_m}{\partial J_\nu}\right)_T\frac{\partial J_\nu}{\partial t} + \left(\frac{\partial E_m}{\partial t}\right)_{J_\nu, T} \tag{3.10}$$

The first term on the right hand side of this expression describes the response of the material energy density to a change in temperature, with fixed radiation densities, while the second term describes the material response to a change in radiation at fixed temperature. The coefficient of the first term can be defined as the non-LTE specific heat, related to the LTE specific heat by

$$c_V^{LTE} = c_V^{NLTE} + \sum_\nu\left(\frac{\partial E_m}{\partial J_\nu}\right)_T\frac{\partial B_\nu}{\partial T}\ ,\ c_V^{NLTE} = \left(\frac{\partial E_m}{\partial T}\right)_{J_\nu} \tag{3.11}$$

The last term arises from evolution of the material at fixed temperature and radiation, and acts as a source or sink of energy. We will consider this term further in Sec. 6, but will neglect it for the remainder of this discussion.

Non-LTE effects become significant at densities low enough so that collisional transition rates no longer dominate the important radiative rates. A numerical example illustrates the relative importance of the temperature

and radiative responses to the specific heat. For this example, we calculate the specific heat of a Kr plasma at three different densities. Figs. 1a - 1c show the specific heat as a function of temperature for ion number densities of 10^{18}, 10^{20} and 10^{22} cm^{-3}, respectively. In each figure, the solid line gives the LTE specific heat, c_V^{LTE}, while the dotted line gives the non-LTE specific heat c_V^{NLTE} evaluated assuming a Planckian radiation field at the given temperature, and the dashed line gives c_V^{NLTE} evaluated assuming no radiation field.

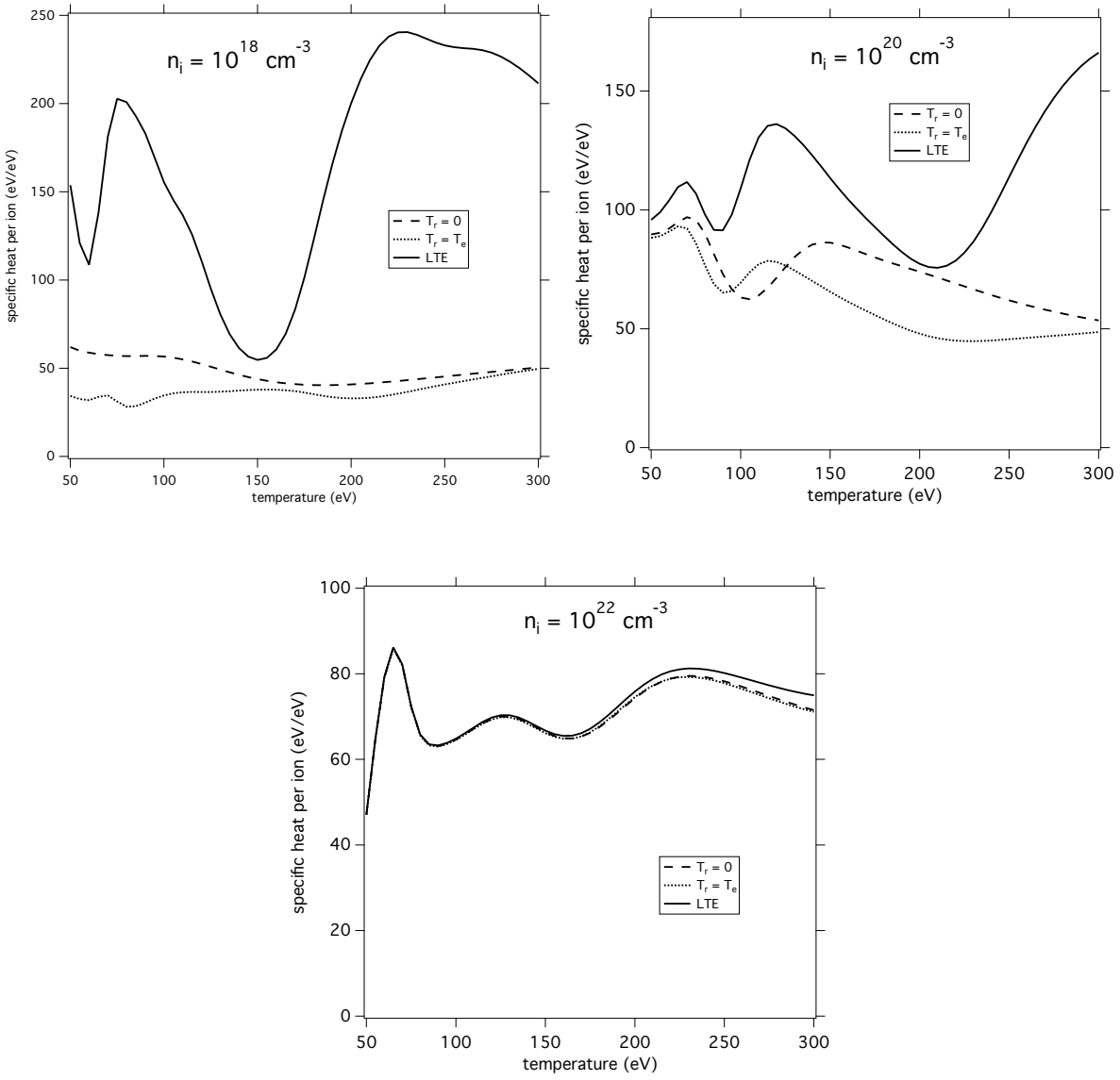

Fig. 1. (a) Specific heat per ion as a function of temperature for a Kr plasma of number density 10^{18} cm^{-3}, in units eV/eV. The solid line gives the LTE specific heat, the dotted line gives the non-LTE specific heat for a Planckian radiation field ($T_r = T_e$, where T_e is the material temperature and T_r is the radiation temperature), and the dashed line gives the non-LTE specific heat with no radiation field ($T_r = 0$). (b) Same as (a) for a number density of 10^{20} cm^{-3}. (c) Same as (a) for a number density of 10^{22} cm^{-3}.

At the highest of the three densities, LTE is a good approximation and the specific heat varies little with the radiation. As the density decreases, the difference between c_V^{LTE} and c_V^{NLTE} increases, and it becomes apparent that the material radiative response dominates the temperature response. Regardless of any other considerations, use of the LTE specific heat at low densities in the presence of non-Planckian radiation fields will not describe the material energetics correctly. Similarly, use of the non-LTE specific heat without accounting for the radiative response will not produce accurate results. Implications of this for radiation transport are discussed in [7].

4. High density effects

a) Ionization Potential Depression

The starting point for almost all CR models is the development of an atomic model for each element, providing both the energy level structure for that element and information needed to calculate transition rates (e.g. oscillator strengths). This data is commonly provided for an "isolated atom", i.e. calculated in the absence of boundaries or neighboring ions. However, the plasma environment affects both the structure and the rates, and these changes must then be incorporated in the evaluation of the CR model rather than in the atomic data. At low densities, the changes are minor and can be incorporated easily. At high densities, the changes are dramatic and impact many aspects of the CR model.

In the "isolated atom" limit of vanishing density, the partition function for a given element (or charge state) becomes infinite, since the atomic levels extend to infinity in principal quantum number, with increasing degeneracy but finite energy. The electrostatic potential due to the presence of free electrons and neighboring ions at a finite density effectively lowers the ionization potential and truncates the partition functions. This phenomenon is referred to as "pressure ionization", "continuum lowering" or "ionization potential depression" (IPD). At low densities, this truncation may happen at higher principal quantum number n than those included in the CR atomic data and the effects are (hopefully) negligible. Under conditions obtained in recent experiments [8], the truncation occurs in the neighborhood of $n \sim 2\text{-}3$. Theoretical modeling of these experimental results is currently an active research area, as extant IPD models are not completely satisfactory for these conditions. For the purpose of this section, we adopt a model and discuss its implementation in a CR model.

A widely-used model for IPD, due to Stewart and Pyatt [9], was described in Chap. 1 and we reproduce the relevant formulas here. An ion of net charge z after ionization (with z=1 for a neutral atom) experiences a reduction in ionization potential of magnitude

$$\Delta E_z = \frac{\left[\left(1+a/\lambda_D\right)^{2/3}-1\right]}{2\left(z^*+1\right)}\ ,\ z^* = \frac{\sum_i z_i^2 N_i}{\sum_i z_i N_i} \tag{4.1}$$

where $z_i = (z\text{-}1)$ is the ion charge, λ_D is the Debye radius and a is the ion sphere radius

$$\lambda_D = \left[\frac{4\pi e^2}{kT}(z^*+1)n_e\right]^{-1/2},\ a = \left(\frac{3z}{4\pi n_e}\right)^{1/3} \tag{4.2}$$

and, for simplicity, we have assumed $T = T_e = T_i$. At low density / high temperature, this expression limits to the Debye-Hückel model, while at high density / low temperature, it limits to the ion sphere model

$$\frac{a}{\lambda_D} << 1 :\ \Delta E_z = \frac{ze^2}{\lambda_D kT} \quad , \quad \frac{a}{\lambda_D} >> 1 :\ \Delta E_z = \frac{3}{2}\frac{ze^2}{akT} \tag{4.3}$$

A straightforward implementation of this in a CR model simply deletes levels in each charge state z that are bound by less than ΔE_z. In practice, several difficulties arise from this simple implementation. The IPD changes the ionization balance by an amount depending on the plasma conditions, so the iterative process of obtaining a self-consistent value for n_e to maintain charge neutrality becomes more complicated. Since the existence of a particular bound state depends discontinuously on n_e, the iterations may oscillate rather than converge. Similar statements apply to constructing derivatives with respect to temperature and electron density, as the energy levels E_i now also depend on the plasma conditions. The derivatives themselves will also be discontinuous, possibly leading to numerical difficulties in the RH code.

We also note that at high enough densities (or low enough temperatures), some charge states may end up with no bound states remaining, with the most neutral charge states disappearing first. Due to the approximate nature of the model, the remaining charge states may not be contiguous under all conditions. This can also lead to erroneous behavior in the CR model if not guarded against. The disappearance of the most neutral charge states at high density and low temperature crudely mimics the formation of nonlocalized conduction bands in metals, but the CR model lacks the necessary physics to transition to a solid state. See [10] for an attempt to link to some aspects of a solid state model.

Allowing the bound states to gradually disappear can ameliorate the discontinuous behavior. Physical justifications for this are the broadening of the level with increased perturbations and fluctuations in the electrostatic potential due to thermal motions of the ions. In practice, the gradual disappearance is achieved by decreasing the degeneracy g_i of level i so that it smoothly vanishes over an appropriate range of densities. Zimmerman and More [11] introduced a simple version of this in the context of an average-atom model. A more comprehensive approach, the occupation probability formalism [12], derives the reduced degeneracies and partition function truncation from contributions of 2-particle interactions to the Helmholtz free energy, ensuring a thermodynamically consistent EOS in LTE. The application of this formalism to non-LTE simulations is discussed in [13].

The interactions that truncate the partition function also imply the existence of additional terms in the expressions for the plasma energy density and pressure. Coulomb interactions between charged particles, in particular, can make significant contributions to these quantities. The connection between reduced degeneracies / occupation probabilities and contributions to the free energy is discussed in [12], with the result that interactions linear in number density do not contribute to the energy density or pressure. This will be approximately true for most interactions in the low-density limit, so we will neglect pressure terms from the reduced degeneracies.

The Coulomb interaction terms can be obtained from the free energy and, in general, provide a negative contribution to the pressure. At low density, using Debye-Hückel theory, the pressure contribution is

$$E_{coul} = -\frac{kT}{8\pi}\frac{1}{\lambda_D^3} = -\frac{1}{2}\frac{e^2}{\lambda_D}(z^*+1)n_e \ , \ P_{coul} = \frac{1}{3}E_{coul} \tag{4.4}$$

An analytical expression for the free energy term that extends this result to include electron degeneracy is presented in [14]. At high densities, the ion sphere limit for Coulomb interactions is

$$E_{coul} = -\frac{9}{10}\frac{e^2}{a}z^* n_e \ , \ P_{coul} = \frac{1}{3}E_{coul} \tag{4.5}$$

Note that at sufficiently high densities, the total pressure can become negative due to the Coulomb term. However, at these densities non-LTE effects in the EOS are liable to be small and using values from a more consistent LTE EOS is likely to be a better option.

b) Electron degeneracy

For thermal electrons described by temperature T_e, the Maxwellian distribution considered so far is only valid at densities low enough so the electrons are not degenerate. Higher densities, or lower temperatures, require use of the Fermi-Dirac distribution, in which the mean occupation of a state of energy ε is given by

$$F_e(\varepsilon) = \frac{1}{1+e^{(\varepsilon-\mu)/kT_e}} \tag{4.6}$$

and the electron distribution function is

$$f_e(\varepsilon) = 4\pi\left(\frac{2m_e}{h^2}\right)^{3/2}\varepsilon^{1/2}F_e(\varepsilon) \tag{4.7}$$

Here, μ is the chemical potential, related to the electron density n_e through

$$n_e = \int_0^\infty d\varepsilon f_e(\varepsilon) = \frac{4}{\sqrt{\pi}}\left(\frac{2\pi m_e kT_e}{h^2}\right)^{3/2} I_{1/2}(\mu/kT_e) \tag{4.8}$$

where I_m is the Fermi-Dirac integral of order m and we have assumed non-relativistic electrons with $\varepsilon = \frac{1}{2}m_e v^2$. In the low-density limit, $-\mu/kT \gg 1$, the chemical potential and electron density are simply related through

$$e^{\mu/kT_e} = \frac{n_e}{2}\left(\frac{h^2}{2\pi m_e kT_e}\right)^{3/2} = \frac{1}{2}n_e\lambda_e^3 \tag{4.9}$$

where λ_e is the electron thermal wavelength.

Transition rates, radiative properties and material properties must all be modified from the formulas used for low-density plasmas. A discussion of the thermodynamics of a degenerate electron gas is available from most textbooks on statistical mechanics, e.g. [15]. For convenience, we quote expressions for the electron energy density and pressure,

$$E_e = n_e kT_e \frac{I_{3/2}(\mu/kT_e)}{I_{1/2}(\mu/kT_e)}\ ,\ P_e = \tfrac{2}{3}E_e \tag{4.10}$$

A result of particular utility for CR models is the Saha equation for degenerate electrons [14]

$$\frac{N_{i+1}}{N_i}e^{\mu/kT_e} = \frac{Z_{i+1}(T_e)}{Z_i(T_e)}e^{-\Delta E/kT_e} \tag{4.11}$$

Since this form of the Saha equation is valid for arbitrary degeneracy, we can use the detailed balance relationships derived for low-density plasmas simply substituting $e^{\mu/kT}$ for each occurrence of $\frac{1}{2}\, n_e\lambda_e^3$.

Including degeneracy, the transition rate for a collisional excitation of energy ΔE becomes

$$C_{ij}^{cx} = \int_{\Delta E}^{\infty} \mathrm{v}(\varepsilon)\sigma_c^{ij}(\varepsilon) f_e(\varepsilon)\left[1 - F_e(\varepsilon - \Delta E)\right] d\varepsilon \tag{4.12}$$

where the integral over the electron distribution now includes a blocking factor $\left[1-F_e\right]$ for the outgoing electron of energy ε-ΔE. Expressing the cross section in terms of the collision strength $\Omega \propto \varepsilon\sigma$ (or equivalently, the Gaunt factor), the transition rate is proportional to the integral

$$I^{cx} = \frac{4}{\sqrt{\pi}}\frac{1}{\lambda_e^3}\int_{\Delta E}^{\infty}\Omega(\varepsilon)\frac{1}{1+e^{(\varepsilon-\mu)/kT_e}}\left[1 - \frac{1}{1+e^{(\varepsilon-\Delta E-\mu)/kT_e}}\right]\frac{d\varepsilon}{kT_e} \tag{4.13}$$

where we have omitted the constants relating Ω and εσ. Since the collision strength varies slowly with energy, we first assume that the collision strength is a constant. The integral can then be done analytically, giving

$$I^{cx} = \frac{4}{\sqrt{\pi}}\frac{\Omega}{\lambda_e^3}\frac{e^{-\Delta E/kT_e}}{1-e^{-\Delta E/kT_e}}\ln\left[\frac{1+e^{\mu/kT_e}}{1+e^{(\mu-\Delta E)/kT_e}}\right] \tag{4.14}$$

while the same integral in the absence of degeneracy gives

$$I_{nd}^{cx} = \frac{4}{\sqrt{\pi}}\frac{\Omega}{\lambda_e^3}e^{(\mu-\Delta E)/kT_e} \tag{4.15}$$

The ratio of these two integrals then provides a "degeneracy factor" which, when multiplied by a non-degenerate transition rate, produces the equivalent transition rate incorporating degeneracy effects

$$\beta^{cx} = \frac{e^{-\mu/kT_e}}{1-e^{-\Delta E/kT_e}}\ln\left[\frac{1+e^{\mu/kT_e}}{1+e^{(\mu-\Delta E)/kT_e}}\right] \tag{4.16}$$

The expression in brackets varies slowly with μ/kT_e, becoming a constant, $\Delta E/kT_e$, in the high-density limit. The transition rate does not increase further with electron density, unlike the non-degenerate case, being restricted by the limiting value of the electron distribution function.

While the collision strength is not strictly constant, small deviations do not affect the degeneracy factor significantly. For collision strengths well approximated by a constant plus a logarithmic term (e.g. Gaunt factors of Mewe [16] or Van Regemorter [17]), the formula underestimates the numerical degeneracy factor by at most a factor of a few while the degeneracy factor itself decreases by ten orders of magnitude. Collision strengths of forbidden transitions tend to vary in leading order as ε^{-1} or ε^{-2} and for these transitions the formula overestimates the degeneracy factor by a similar factor. If higher accuracy is desired, numerical integrations corresponding to $\ln(\varepsilon)$ and ε^{-n} terms could provide slowly varying corrections to the above degeneracy factor.

A collisional ionization of energy ΔE produces two outgoing electrons of energy ε' and ε-ε'-ΔE and the transition rate integral contains blocking factors for both electrons

$$C_{ij}^{ci} = \int_{\Delta E}^{\infty} d\varepsilon \, \mathrm{v}(\varepsilon) f_e(\varepsilon) \int_0^{\Delta E} d\varepsilon' \sigma_c^{ij}(\varepsilon,\varepsilon') \left[1 - F_e(\varepsilon')\right] \left[1 - F_e(\varepsilon - \varepsilon' - \Delta E)\right] \tag{4.17}$$

Assuming that the differential cross section $\sigma(\varepsilon,\varepsilon')$ is independent of ε' and that the collision strength is independent of ε leads to a degeneracy factor for collisional ionization rates of

$$\beta^{ci} = e^{-(\mu-\Delta E)/kT_e} \int_{\Delta E}^{\infty} \frac{d\varepsilon}{1+e^{(\varepsilon-\mu)/kT_e}} \frac{1}{(\varepsilon - \Delta E)} \int_0^{\varepsilon-\Delta E} \frac{d\varepsilon'}{kT_e} \left[1 - \frac{1}{1+e^{(\varepsilon-\varepsilon'-\mu)/kT_e}}\right] \left[1 - \frac{1}{1+e^{(\varepsilon-\varepsilon'-\Delta E-\mu)/kT_e}}\right] \tag{4.18}$$

The double integral cannot be done analytically, but the expression

$$\beta^{ci} \approx \zeta \beta^{cx} \;,\; \zeta = \ln\left(1 + e^{-\mu/kT_e}\right) \tag{4.19}$$

provides a very good approximation over a wide range of parameters. Fig. 2 presents these degeneracy factors for a transition with $\Delta E/kT_e = 1$. Choosing a different value of $\Delta E/kT_e$ shifts the curves slightly in μ/kT_e, but does not change their character.

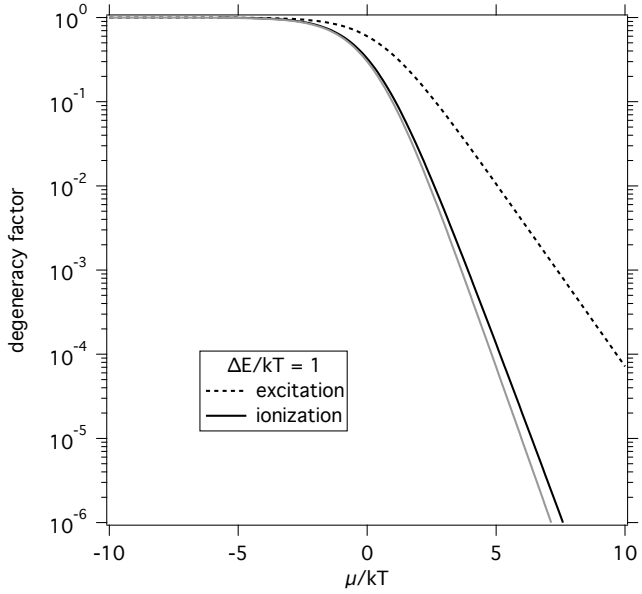

Fig. 2. Degeneracy factors for a transition with $\Delta E/kT = 1$. The dashed line gives the degeneracy factor for excitation β^{cx}. The solid black line gives the degeneracy factor for ionization β^{ci} from Eq. (4.19). The solid gray line gives β^{ci} from a numerical evaluation of Eq. (4.18).

The degeneracy factor for ionization drops more sharply with increasing μ/kT_e than the factor for excitation, due to the presence of blocking factors for both outgoing electrons. The main approximation here is the assumption that the differential cross section is independent of the outgoing electron energy. However, numerical integrations using a more realistic differential cross section [18] give results that are virtually indistinguishable from those obtained with a differential cross section independent of ε'.

Electron degeneracy also affects other transitions that involve free electrons. Photoionization produces a single outgoing free electron and requires an appropriate blocking factor, decreasing the absorption coefficient for photons close to threshold energy. Autoionization transitions should be treated in a similar manner, although the emitted electrons tend to be of relatively high energy and minimally affected by degeneracy.

More important are transitions between free electron states, i.e. bremsstrahlung and inverse bremsstrahlung, which do not affect the bound state distributions but can be critical in determining the energy balance of a dense radiating plasma. The effects of degeneracy on these absorption and emission processes have been discussed in the literature in varying levels of detail, e.g. [19-20], but can be understood in terms of the previous discussion. Each such (absorption) transition involves a single incoming electron of energy ε and a single outgoing electron of energy ε-$h\nu$, with a cross-section inversely proportional to electron velocity (incorporating various quantum effects into a

Gaunt factor). Accordingly, under the assumption of a constant Gaunt factor, the degenerate and non-degenerate treatments differ by the factor β^{cx}, with the substitution of $h\nu$ for ΔE. We note that plasma collective effects can also strongly affect radiative properties [21] and assume that these effects can be treated independently.

5. Detailed balance, energy conservation and discretization

The principle of detailed balance is used extensively in CR modeling to relate forward and inverse rates, ensuring that the CR model does indeed produce an equilibrium atomic population distribution when driven by thermal photon and electron distributions. As discussed in Section 2, Kirchoff's law, relating the radiative emission and absorption coefficients in LTE, is a corollary of this principle and ensures that there is no net energy transfer between radiation and matter when the radiation is also in equilibrium with the matter. However, the numerical realization of Kirchoff's law and, separately, total energy conservation depend on the discretization of the radiation field and the atomic levels.

The numerical issues can be demonstrated by considering a single radiative excitation / de-excitation, as the ratio of emission and absorption coefficients for each transition must also obey Kirchoff's law. Using the expressions for absorption and emission coefficients from Section 2b and assuming a Boltzmann distribution of excited states results in a source function

$$S_\nu^{ij} = \frac{2h\nu^3}{c^2}\frac{\frac{g_i}{g_j}y_j}{y_i - \frac{g_i}{g_j}y_j} = \frac{2h\nu^3}{c^2}\frac{1}{e^{E_{ij}/kT_e}-1} \tag{5.1}$$

which is equal to the Planck function only for $h\nu = E_{ij}$. This discrepancy is not due to an assumption of a narrow line profile, but instead comes from treating the energy levels as monoenergetic. Since the cross section is not a delta function, a photon of energy $h\nu$ can induce a transition of energy $E_{ij} \neq h\nu$. The consequences of this inconsistency become more significant as line profiles become wider, due to either increasing density or the use of statistical treatments such as unresolved transition arrays (UTA). A similar discrepancy will occur for radiative ionization / recombination transitions if the threshold photon energy does not match the transition energy.

A physically motivated, but expensive, remedy would be to treat each energy level as having a finite width, dividing it into sublevels. This approach would allow (or require) including those (near-) elastic collisions that distribute populations within the energy level (as is done in some treatments of partial redistribution [6]). Fortunately, the correct LTE source function can be obtained by slightly modifying the emission coefficient from that given in Eq. (2.14) to account for the mismatch between the photon energy and the transition energy:

$$\eta_\nu^{ij} = \left(\frac{e^{E_{ij}/kT_e}-1}{e^{h\nu/kT_e}-1}\right)\frac{2h\nu^3}{c^2}\frac{g_i}{g_j}\sigma_\nu^{ij} \tag{5.2}$$

The total source function calculated in this manner will match the Planck function when the populations have a thermal distribution.

This can be a critical issue when driving thermal radiation transport with a CR model under near-LTE conditions. Fig. 3 shows the source functions obtained with a screened-hydrogenic atomic model for Kr that uses superconfigurations and UTAs [22]. The CR model was evaluated in LTE for a material temperature of 100 eV and an ion number density of 10^{18} cm^{-3}. The solid line was obtained with uncorrected emission coefficients, while the dashed line used Eq. (5.2) and is indistinguishable from the Planck function. A measure of the inconsistency is given by frequency-integrating the source function, which for the uncorrected case is only 84% of the integrated Planck function. This produces a gross imbalance in the material energy equation, leading to incorrect material temperatures. Figure 4 shows the steady-state material temperature obtained by integrating the material energy equation, as a function of radiation temperature for the same number density.

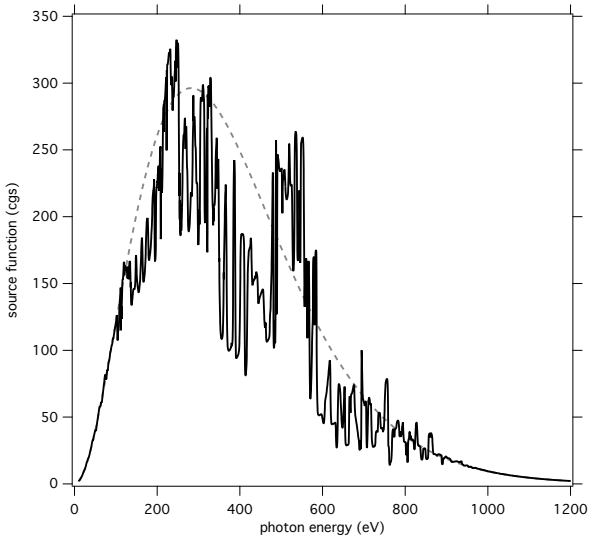

Fig. 3. Source function for a Kr plasma with T_e = 100 eV and $n_i = 10^{18}$ cm^{-3}. The solid line was obtained with uncorrected emission coefficients from Eq. (5.1), while the dashed line used Eq. (5.2).

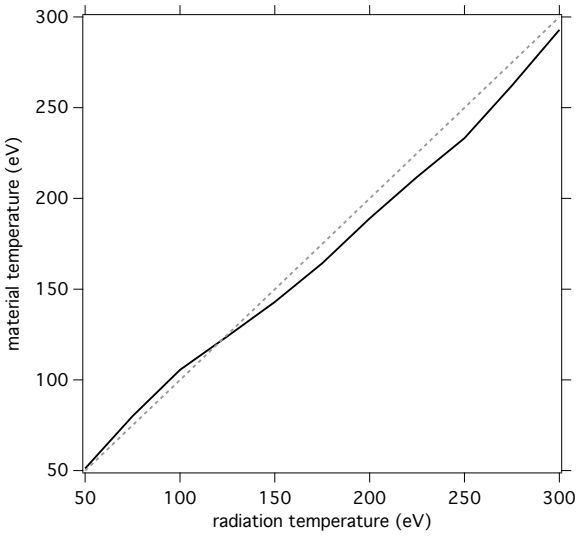

Fig. 4. Steady-state material temperature obtained from material energy equation as a function of radiation temperature using uncorrected emission coefficients. The dashed line gives $T_e = T_r$ as a reference.

While this expression can be applied directly to the emission at any given frequency, energy equilibrium is a statement about frequency-integrated emission and absorption. To analyze that, we must consider the discretized radiation field as used in both the CR model and in the radiation transport. We assume a multigroup description of the radiation field and denote a quantity X that has been averaged over group g as X_g, e.g. the intensity averaged over the group is given by

$$J_g = \frac{1}{\nu_g - \nu_{g-1}} \int_{\nu_{g-1}}^{\nu_g} J_\nu \, d\nu \tag{5.3}$$

The discretized material energy equation becomes

$$\frac{dE_m}{dt} = 4\pi \sum_g \alpha_g \left(J_g - S_g \right) (\nu_g - \nu_{g-1}) \tag{5.4}$$

Evaluating this in equilibrium with $J_\nu = B_\nu$, then each summand must be zero, giving the result for the discretized emission coefficient

$$\eta_g^{ij} = \left(\frac{e^{E_{ij}/kT_e} - 1}{e^{h\nu/kT_e} - 1} \right) \frac{g_i}{g_j} \sigma_\nu^{ij} B_g \tag{5.5}$$

These modifications to the emission coefficients ensure the correct equilibrium behavior, but they are not sufficient to guarantee energy conservation away from equilibrium. The underlying cause is the possible mismatch between the average photon energy in the radiation transport and the transition energy. For a single radiative excitation, each transition increases the material energy by E_{ij} while the radiation energy decreases by $h\nu_g$. Multiplying both the absorption and emission coefficients by $E_{ij} / h\nu_g$ restore energy conservation. In most cases, this correction is very small. However, it can become significant if, for efficiency or accuracy purposes, transition energies do not correspond to the level energies.

One additional degree of freedom in the connection between the CR model and radiation transport is that the definition of J_g does not uniquely specify the values of J_ν within group g to be used for calculating transition rates. This can be used to e.g. drive low-energy transitions with a better representation of a Planckian than would otherwise be possible with a small number of groups. If J_ν differs from J_g, then the aforementioned correction must be modified to maintain energy conservation.

6. Conservation and consistency in non-LTE thermal radiation transport

The material presented in the previous section applies to the CR model and is primarily aimed at achieving equilibrium information for use in thermal radiation transport. We now consider the more general non-equilibrium case, with the emphasis again on the material energy equation. In the following, the mass density is kept fixed and, for simplicity, we refer to a single material temperature T.

The goal for radiation transport is to obtain a self-consistent solution of the radiation transport equation and the material energy equation. Most transport algorithms used in RH codes assume that LTE holds and exploit that assumption to efficiently provide a consistent solution in terms of the material temperature. Consistency, as used here, means that the solution satisfies both equations when evaluated with updated temperatures and intensities. The solution will also conserve energy if the change in material energy density, as obtained by evaluating the EOS at the given temperature, matches the change in energy given by the material energy equation. The system of equations is both nonlocal and nonlinear in temperature, but many effective solution methods are available.

Our concern here is not the solution method, but the treatment of the material energy equation. For simplicity, we adopt a simple time-discretization:

$$E_m(T^1) - E_m(T^0) = 4\pi\,\Delta t \int \alpha_\nu (J_\nu^1 - B_\nu(T^1))\,d\nu \tag{6.1}$$

where the superscript "0" refers to the beginning of the timestep and the superscript "1" refers to the end of the timestep. The prevalent approach to solving this set of equations uses a temperature expansion in the form

$$c_V^{LTE}(T^* - T^0) = 4\pi\,\Delta t \int \alpha_\nu \left(J_\nu^* - B_\nu(T^0) + \frac{\partial B_\nu}{\partial T}(T^* - T^0)\right) d\nu \tag{6.2}$$

where the superscript "*" refers to an intermediate temperature. The solution procedure solves for J_ν^* and T^*, updates the source function, and repeats. Successive iterations should approach J_ν^1 and T^1 as (and if) the algorithm converges. Using the specific heat to express the change in material temperature introduces an error into the energy balance, as the iterations actually converge to

$$c_V^{LTE}(T^1 - T^0) = 4\pi\,\Delta t \int \alpha_\nu (J_\nu^1 - B_\nu(T^1))\,d\nu \tag{6.3}$$

instead of Eq. (6.1). In most cases, this error is small. In LTE, evaluating the EOS at the beginning of each iteration to update the material energy leads to

$$c_V^{LTE}(T^1 - T^*) + E_m(T^*) - E_m(T^0) = 4\pi\,\Delta t \int \alpha_\nu \left(J_\nu^1 - B_\nu(T^*) + \frac{\partial B_\nu}{\partial T}(T^1 - T^*)\right) d\nu \tag{6.4}$$

which does converge to Eq. (6.1).

This formulation explicitly uses the fact that the both the material energy density and source function (which in LTE is the Planck function) are dependent only on the temperature. When LTE does not hold, then both the material energy density and source function (or emission coefficient) also depend on the intensity. An equivalent approach to that described above would use derivatives with respect to intensity as well as temperature, e.g.

$$S_\nu(T^*, J_\nu) \approx S_\nu(T^0, J_\nu{}^0) + \frac{\partial S_\nu}{\partial T}(T^* - T^0) + \sum_{\nu'} \frac{\partial S_\nu}{\partial J_{\nu'}}(J_{\nu'} - J_{\nu'}{}^0) \tag{6.5}$$

but requires significant changes to the radiation transport. Ignoring the radiation response terms and using an expansion in temperature (with a non-LTE source function), such as

$$c_V^{NLTE}(T^* - T^0) = 4\pi\,\Delta t \int \alpha_\nu [J_\nu - S_\nu(T^*) - \frac{\partial S_\nu}{\partial T}(T^* - T^0)]\,d\nu \tag{6.6}$$

may work but will not conserve energy, as the left hand side of this equation is no longer the change in material energy and the right hand side is no longer the change in radiation energy.

As discussed in section 3, even if the conditions are in (or close to) LTE, the non-LTE specific heat can be much smaller than the LTE specific heat, leading to large temperature excursions or even divergence. A similar difficulty arises from expanding the source function (or emission coefficient). If the source function is close to a Planck function, using the temperature derivative without accounting for the material response to radiation may destabilize the solution algorithm. These issues are discussed in [7] and an ansatz designed for use under near-LTE conditions is proposed in [22].

One further difference from the LTE case arises from the fact that the material energy density itself is obtained from a time evolution of the CR system. We must now distinguish three values of the energy density: E_m^0 at the beginning of the CR calculation, E_m^1 at the end of the CR calculation (and the beginning of the radiation transport) and E_m^2 at the end of the radiation transport. Both E_m^0 and E_m^1 are evaluated at the initial temperature T^0, with the difference between them due to evolution at fixed temperature, density and radiation intensity. The material energy equation becomes

$$E_m^{\,2} - E_m^{\,1} = 4\pi\,\Delta t \int (\alpha_\nu J_\nu - \eta_\nu)\, d\nu + (E_m^{\,0} - E_m^{\,1}) \tag{6.7}$$

where the last term, E_m^0-E_m^1, is an energy source (or sink) corresponding to the time derivative $\left(\partial E_m / \partial t\right)_{J_\nu, T}$.

As in the LTE case, the energy errors can be reduced by repeated evaluations of the CR model to update the material energy and the source function. As the solution converges, the neglected terms decreases in importance. This approach can be computationally expensive, but even a single iteration may improve the solution significantly.

These considerations have proven to be significant in RH simulations of indirectly driven inertial confinement fusion (ICF) capsules on the National Ignition Facility. Achieving energy production from a capsule requires a finely tuned implosion and energy conservation in the simulation is critical. Conditions in the DT-filled plastic capsule near the ablation surface are very close to LTE. Fig. 5 presents the energy production rate as a function of time obtained from a simulation using four different treatments of the radiation transport. The production rates have been normalized relative to the total energy produced in the reference case and the time is relative to the peak production rate of the same case. The reference case assumed the material remained in LTE. The simulation for curve A changed the temperatures to conserve energy, while the simulation for curve B used the temperatures as obtained from the radiation transport. The simulation for curve C evaluated the CR model with updated temperatures and intensities and re-evaluated the radiation transport one time to obtain a more consistent set of temperatures and material energy densities. All curves are labeled with the total energy produced, relative to the LTE simulation. Differences between each pair of curves are experimentally significant.

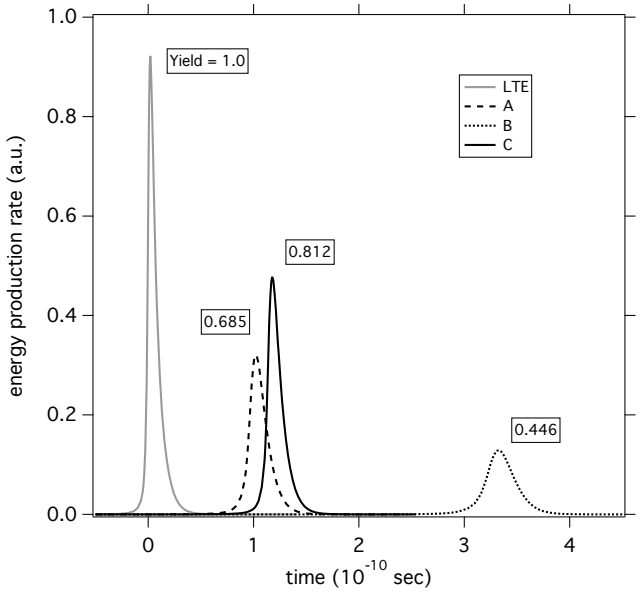

Fig. 5. Relative energy production rate as a function of time for a simulated ICF capsule implosion. The gray curve shows the result obtained assuming LTE. Curve A changed temperatures to conserve energy, while curve B used the temperatures as obtained from the radiation transport. Curve C evaluated the CR model with updated temperatures and intensities. All curves are labeled with the total energy produced, relative to the LTE simulation.

7. Summary

Employing a collisional-radiative model in a radiation hydrodynamics code requires modifying the usual formalism. Simulations require both material properties and response functions. Providing information for the high densities that may be encountered in a simulation requires including ionization potential depression and electron degeneracy. Maintaining energy conservation puts constraints on the discretized equations. These requirements can be met through straightforward modifications to the CR system, extending the range of a radiation hydrodynamics code to conditions that are far from LTE.

Acknowledgments

The author gratefully acknowledges many enlightening conversations with George Zimmerman and John Castor.

This work performed under the auspices of U.S. Department of Energy by Lawrence Livermore National Laboratory under Contract DE-AC52-07NA27344.

References:

1. H.-K. Chung, M.H. Chen, W.L. Morgan, Y. Ralchenko, R.W. Lee, HEDP **1**, 3-12 (2005).
2. J. Abdallah, Jr., G. Csanak, Y. Fukuda, *et al*, Phys. Rev. **A68**, 063201 (2003).
3. G. Colonna, L.D. Pietanza, M. Capitelli, Spectrochim. Acta Part B **56**, 587-598 (2001).
4. M.E. Sherill, J. Abdallah, Jr., G. Csanak, *et al*, JQSRT **99**, 584-594 (2006).
5. A.G. de la Varga, P. Velarde, F. de Gaufridy, *et al*, HEDP **9**, 542-547 (2013).
6. J. Oxenius, *Kinetic Theory of Particles and Photons*, Springer-Verlag, 1986.
7. H. Scott, HEDP **1**, 31-41 (2005).
8. O. Ciricosta, S.M. Vinko, H.-K. Chung, *et al*, Phys. Rev. Lett. **109**, 065002 (2012)
9. J.C. Stewart, K.D. Pyatt, Astrophys. J. **144**, 1203-1211 (1966).
10. B. Deschaud, O. Peyrusse, F.B. Rosmej, HEDP **15**, 22-29 (2015).
11. G.B. Zimmerman and R.M. More, JQSRT **23**, 517-522 (1980).
12. D.G. Hummer and D. Mihalas, Astrophys. J. **331**, 794-814 (1988).
13. I. Hubeny, D.G. Hummer and T. Lanz, Astron. Astrophys. **282**, 151-167 (1994).
14. H.C. Graboske, D.J. Harwood and F.J. Rogers, Phys. Rev. **186**, 210-225 (1969).
15. R.K. Pathria, *Statistical Mechanics*, Pergamon Press, 1972.
16. R. Mewe, Astron. & Astrophys. **20**, 215-221 (1972).
17. H. Van Regemorter, Astrophys. J. **136**, 906-915 (1992)
18. R.E.H. Clark, J. Abdallah, Jr., J.B. Mann, Astrophys J **381**, 597-600 (1991).
19. H. Totsuji, Phys. Rev. **A32**, 3005-3010 (1985).
20. S. Eliezer, P.T. Leon, J.M. Martinez-Val and D.V. Fisher, Laser and Particle Beams **21**, 599-607 (2003).
21. G. Bekefi, *Radiation Processes in Plasmas*, John Wiley & Sons, 1966.
22. H.A. Scott and S.B. Hansen, HEDP **6**, 39 (2010).